

Article

SPAG9 Expression Predicts Good Prognosis in Patients with Clear-Cell Renal Cell Carcinoma: A Bioinformatics Analysis with Experimental Validation

Liwen Qiao, Lu Zhang and Huiming Wang * 

Department of Nephrology, Renmin Hospital of Wuhan University, Wuhan 430060, China; qiaoliwen2021@163.com (L.Q.)

* Correspondence: rm000301@whu.edu.cn; Tel.: +86-18971563100

Abstract: Clear-cell renal cell carcinoma (ccRCC) is the most common and aggressive type of renal-cell carcinoma (RCC). Sperm-associated antigen 9 (*SPAG9*) has been reported to promote the progression of a variety of tumors and is thus a potential prognostic marker. This study combined a bioinformatics analysis with an experimental validation, exploring the prognostic value of *SPAG9* expression in ccRCC patients and the possible underlying mechanisms. The *SPAG9* expression was associated with a poor prognosis in pan-cancer patients, but with a good prognosis and slow tumor progression in ccRCC patients. To explore the underlying mechanism, we investigated the roles of *SPAG9* in ccRCC and bladder urothelial carcinoma (BLCA). The latter was chosen for comparison with ccRCC to represent the tumor types in which *SPAG9* expression suggests a poor prognosis. The overexpression of *SPAG9* increased the expression of autophagy-related genes in 786-O cells but not in HTB-9 cells, and *SPAG9* expression was significantly correlated with a weaker inflammatory response in ccRCC but not in BLCA. Through an integrated bioinformatics analysis, we screened out seven key genes (*AKT3*, *MAPK8*, *PIK3CA*, *PIK3R3*, *SOS1*, *SOS2*, and *STAT5B*) in this study. The correlation between *SPAG9* expression and ccRCC prognosis depends on the expression of key genes. Since most of the key genes were PI3K-AKT-pathway members, we used the PI3K agonist 740Y-P to stimulate the 786-O cells, to mimic the effect of key-gene overexpression. Compared with the Ov-*SPAG9* 786-O cells, the 740Y-P further increased the expression of autophagy-related genes by more than twofold. Moreover, we constructed a nomogram based on *SPAG9*/key genes and other clinical features, which was proven to have some predictive value. Our study found that *SPAG9* expression predicted opposite clinical outcomes in pan-cancer and ccRCC patients, and we speculated that *SPAG9* suppresses tumor progression by promoting autophagy and inhibiting inflammatory responses in ccRCC. We further found that some genes might cooperate with *SPAG9* to promote autophagy, and that these were highly expressed in the tumor stroma and could be represented by key genes. The *SPAG9*-based nomogram can help to estimate the long-term prognosis of ccRCC patients, indicating that *SPAG9* is a potential prognostic marker for ccRCC.

Keywords: *SPAG9*; autophagy; inflammation; clear cell renal carcinoma; nomograms

Citation: Qiao, L.; Zhang, L.; Wang, H. *SPAG9* Expression Predicts Good Prognosis in Patients with Clear-Cell Renal Cell Carcinoma: A Bioinformatics Analysis with Experimental Validation. *Genes* **2023**, *14*, 944. <https://doi.org/10.3390/genes14040944>

Academic Editors: Kenta Nakai, Tun-Wen Pai, Brunella Franco and Stefano Lonardi

Received: 30 November 2022

Revised: 5 April 2023

Accepted: 15 April 2023

Published: 20 April 2023



Copyright: © 2023 by the authors. Licensee MDPI, Basel, Switzerland. This article is an open access article distributed under the terms and conditions of the Creative Commons Attribution (CC BY) license (<https://creativecommons.org/licenses/by/4.0/>).

1. Introduction

Renal cell carcinoma (RCC) is the most common adult renal malignancy, of which the most common and aggressive histologic type is clear-cell renal cell carcinoma (ccRCC). Clear-cell renal cell carcinoma is characterized by abundant glycogen and lipids in the cytoplasm, accounting for 80–90% of RCC cases [1]. The incidence of ccRCC has increased steadily in recent decades, and due to its lack of specific clinical manifestations, nearly one-third of ccRCC patients have already developed distant metastasis at the time of diagnosis and, thus, missed the best opportunity for surgery [2]. Clear-cell renal cell carcinoma is insensitive to chemotherapy or radiotherapy, and although molecular targeted therapies

have been widely used in patients with advanced ccRCC, most patients develop drug resistance after 5–11 months [3]. Therefore, it is necessary to investigate the molecular mechanisms underlying the occurrence and development of ccRCC and to develop potential therapeutic targets and prognostic markers.

Sperm-associated antigen 9 (*SPAG9*) is a cancer-testis antigen expressed in various tumor tissues, which has two main alternative spliceosomes—JLP (1307 amino acids) and SPAG9 (766 amino acids). It plays a wide role in tumor-cell lines: it not only promotes proliferation, migration, and epithelial–mesenchymal transition (EMT) [4–17], but also regulates autophagy [18,19]. A previous study found that *SPAG9* overexpression promotes proliferation and migration in the ccRCC cell lines Caki-1 and NII-AKS413 [4]; however, studies on the prognostic value of *SPAG9* in ccRCC patients are still lacking.

This study combined a bioinformatics analysis and experimental validation, exploring the prognostic value of *SPAG9* expression in ccRCC patients and the possible underlying mechanisms, and constructed a *SPAG9*-based ccRCC prognostic model to help with risk stratification.

2. Materials and Methods

2.1. Data Acquisition

The RNA-seq data and clinical data of ccRCC patients were downloaded from the TCGA database (<https://portal.gdc.cancer.gov/> accessed on 15 June 2022). Gene expression was shown as FPKM (fragments per kilobase of transcript per million mapped fragments). The clinical data included age, gender, pathological grade (G1~G4), clinical stage (Stage I~Stage IV), T stage (tumor size, T1~T4), N stage (tumor lymph-node metastasis, N0~N1), and M stage (tumor distant metastasis, M0~M1). The clinical data of ccRCC included 537 patients, 526 of whom had complete and valid survival information (survival time and vital status), for Kaplan–Meier survival analysis, and 515 of whom had complete and valid survival information and clinical information (age, gender, pathological grade and clinical stage), for Cox regression analysis.

We also obtained RNA-seq data and clinical data of ccRCC from the ICGC database (<https://dcc.icgc.org/> accessed on 15 June 2022): RECA-EU, including 91 patients with complete and valid survival information (survival time and vital status) and clinical information (age, gender). Basic information of the ccRCC patients from the TCGA database and the ICGC database is shown in Tables S1 and S2.

The scRNA-seq data were obtained from the GEO database (<https://www.ncbi.nlm.nih.gov/geo/> accessed on 1 June 2022). Two ccRCC samples (GSM4630028 and GSM4630028) and one normal kidney-tissue sample (GSM4630031) were derived from the GSE152938 dataset, with a reading depth of 10× Genomics based on HiSeq X Ten (Illumina, San Diego, CA, USA) [20]. All 3 scRNA-seq samples were from human organisms.

2.2. Analysis with the Online Tool

The GEPIA2 is an online analysis tool developed by Tang et al., based on the data from the TCGA database (<http://gepia2.cancer-pku.cn/> accessed on 15 June 2022) [21]. Some of the survival curves were established by GEPIA2: after entering gene names, median gene expression was selected as the group cutoff, and the overall survival (OS) rate of the 2 groups was compared by log-rank test. The online tool calculated the hazard ratios (HRs) based on the Cox PH Model, and 95% confidence interval (95% CI) was shown as dotted lines in the pictures. Axis units were set to months. Some correlation analyses were also performed by GEPIA2: after entering gene names, and Pearson’s correlation coefficient between the expressions of genes was calculated.

2.3. Cell Culture and RNA Transfection

The human ccRCC cell line 786-O and BLCA cell line HTB-9 were provided by the American Type Culture Collection (ATCC, Manassas, VA, USA). Cells were cultured in DMEM-F12 medium containing 10% fetal bovine serum (FBS) and kept at 37 °C in a cell incubator with 5% CO₂ and 95% air. Overexpression of *SPAG9* (Ov-*SPAG9*) and overex-

pression control (Ov-NC) were synthesized by RIBIO (Guangzhou, China). Transfection was carried out using Lipofectamine 3000 (Invitrogen, Waltham, MA, USA), following the manufacturer's protocol. After 48 h, the transfection efficiency was detected by real-time quantitation PCR (RT-qPCR). In addition, 786-O cells were treated with the PI3K agonist 740Y-P (20 μ M; MedChemExpress, Monmouth Junction, NJ, USA) for 48 h.

2.4. RNA Extraction and RT-qPCR Assay

Total RNA from cells was extracted using TRIzol reagent (Invitrogen) and reverse-transcribed into cDNA using a RevertAid cDNA Synthesis Kit (Thermo Fisher Scientific, Waltham, MA, USA). The RT-qPCR was performed with SYBR Green PCR Master Mix (Illumina), according to the manufacturer's instructions. Relative mRNA levels were measured with the aid of the $2^{-\Delta\Delta C_t}$ method and standardized to GAPDH. The primer sequences and the qPCR data are shown in Tables S3 and S4.

2.5. GSEA and ssGSEA Analysis

Gene set enrichment analysis (ssGSEA) algorithm was used to evaluate the inflammatory response, inflammatory factor production, and T-cell-exhaustion levels in ccRCC and BLCA samples. The gene set "GOBP_INFLAMMATORY_RESPONSE" from the Molecular Signatures database (<http://www.gsea-msigdb.org/gsea/msigdb/index.jsp/> accessed on 15 June 2022) was used to score the inflammatory response. Inflammatory factors that promote tumor progression (*CRP*, *IL1A*, *IL1B*, *IL6*, *TNF*, *TGFB*, *VEGFA*, *VEGFB*, *VEGFC*, *CXCL1*, *CXCL2*, *MMP2*, and *MMP9*) were used to score inflammatory factor production [22]; T-cell-exhaustion markers (*PDCD1*, *TOX*, *CXCL13*, *TIGIT*, *CTLA4*, *TNFRSF9*, *HAVCR2*, and *LAG3*) were used to score T-cell exhaustion [23].

Gene set enrichment analysis (GSEA) software (version 4.0.3) was used to identify pathways related to *SPAG9* [24,25]. The target set "C2.cp.kegg.v7.5.1.symbols.gmt" was downloaded from the Molecular Signatures database. The false discovery rate p value (FDR p value) and normalized enrichment score (NES) were used as screening criteria, and pathways with $|\text{NES}| > 2$ and FDR p values ≤ 0.05 were considered to be significantly enriched. Genes that contribute to the enrichment score (ES) of a particular pathway are called core enrichment genes, i.e., the leading-edge subset. According to the official description of GSEA, these genes can be interpreted as the core of a pathway and are, therefore, biologically important [25]. Based on the core enrichment genes of each pathway, we used the single-sample gene set-enrichment analysis (ssGSEA) algorithm to evaluate the pathway activity in samples.

2.6. Analysis with R Software

The R software (version 3.5.1) with the packages survival and survminer was used for the survival analysis. The Kaplan–Meier method was used to plot the survival curve, and log-rank was set as the statistical significance test. In Cox regression analysis, HRs were calculated based on the Cox PH Model. In the process of digitizing gender data, "female" was set as 0 and "male" was set as 1. Packages ggplot2 and ggpubr were used for the boxplots; Wilcoxon rank sum was set as the statistical significance test. The ratio of immune and stromal components in tumor samples was calculated by the ESTIMATE algorithm [26]. The heatmaps were plotted with the package Pheatmap. Correlation analysis was performed with the cor() function; Pearson's correlation test served as the statistical significance test.

2.7. ScRNA-seq Data Processing

The ScRNA-seq data were initially processed by the package Seurat in R software. The percentage of mitochondrial genes was calculated by the PercentageFeatureSet() function. The correlations between sequencing depth and mitochondrial gene sequences and between sequencing depth and total intracellular sequences were calculated. Genes detected in <3 cells, cells with <200 total detected genes, cells with <50 sequencing numbers, and cells

with $\geq 5\%$ mitochondrial gene sequences were excluded. After filtering, LogNormalize() was used to normalize the data; FindVariableFeatures() was used to identify the top 1500 hypervariable genes. Principal component analysis (PCA) was performed, and under the condition of p value < 0.05 , dimensions with significant separation were screened out [27]. The 20 principal components (PCs) were selected for secondary dimensionality reduction through the tSNE algorithm [28]. Marker genes in each cell population were identified with the criteria of $|\log_2[\text{fold change(FC)}]| > 1$ and p value < 0.05 . Cell populations were annotated by the package SingleR and manually corrected with the CellMarker database (<http://biocc.hrbmu.edu.cn/CellMarker/index.jsp/> accessed on 15 June 2022) based on the marker genes [29,30]. Pseudotime trajectories were constructed by the package Monocle2; annotated cell populations were positioned to specific locations [31].

2.8. Prognostic Model Construction and Validation

The TCGA cohort (515 patients) was set as the training cohort for constructing the prognostic model, and the ICGC cohort (91 patients) was set as the validation cohort for external validation. The RiskScore was constructed with lasso regression using the R package glmnet [32]. $\text{RiskScore} = \text{ExpGENE1} \times \beta_1 + \text{ExpGENE2} \times \beta_2 + \dots + \text{ExpGENEn} \times \beta_n$, in which “Exp” represents the expression level of the corresponding gene and “ β ” represents the regression coefficient calculated by multivariate Cox analysis [33]. Age, gender, and RiskScore were utilized to construct the nomogram by using the R package rms. Calibration plots were constructed to evaluate the predictive abilities of the nomograms; the number of resampling was 1000 [34]. The receiver operating characteristic (ROC) curves were plotted using the R package timeROC. Time-dependent C-indexes were calculated and plotted using the pec package.

2.9. Statistical Significance

A p value < 0.05 was considered statistically significant.

3. Results

3.1. SPAG9 Expression Suggests Poor Prognosis in Pan-Cancer Patients but Good Prognosis in ccRCC Patients

First, we explored the relationship between SPAG9 expression and the clinical outcomes of the ccRCC patients. In ccRCC, the SPAG9 expression was significantly associated with good prognosis (Figure 1A). Reduced SPAG9 expression was significantly associated with clinical-stage progression (Stage I vs. Stage IV), primary tumor enlargement (T1 vs. T4), and tumor metastasis (N0 vs. N1 and M0 vs. M1) in the ccRCC patients (p value < 0.05 , Figure 1B). The univariate Cox analysis showed that age (HR = 1.029, 95% CI = 1.016~1.043), pathological grade (HR = 2.286, 95% CI = 1.862~2.807), and clinical stage (HR = 1.897, 95% CI = 1.660~2.167) were risk factors for OS in ccRCC patients, and that SPAG9 expression (HR = 0.939, 95% CI = 0.909~0.971) was a protective factor. The multivariate Cox analysis showed that age (HR = 1.030, 95% CI = 1.015~1.045), pathological grade (HR = 1.482, 95% CI = 1.176~1.867), and clinical stage (HR = 1.663, 95% CI = 1.426~1.938) were independent risk factors for OS in the ccRCC patients (p value < 0.05 , Figure 1C).

In pan-cancer, SPAG9 expression was significantly associated with poor prognosis (Figure 2A). In all the tumor types except for ccRCC, SPAG9 was significantly correlated with OS in adrenocortical carcinoma (ACC), BLCA, and kidney chromophobe carcinoma (KICH), and it was a risk factor (Figure 2B).

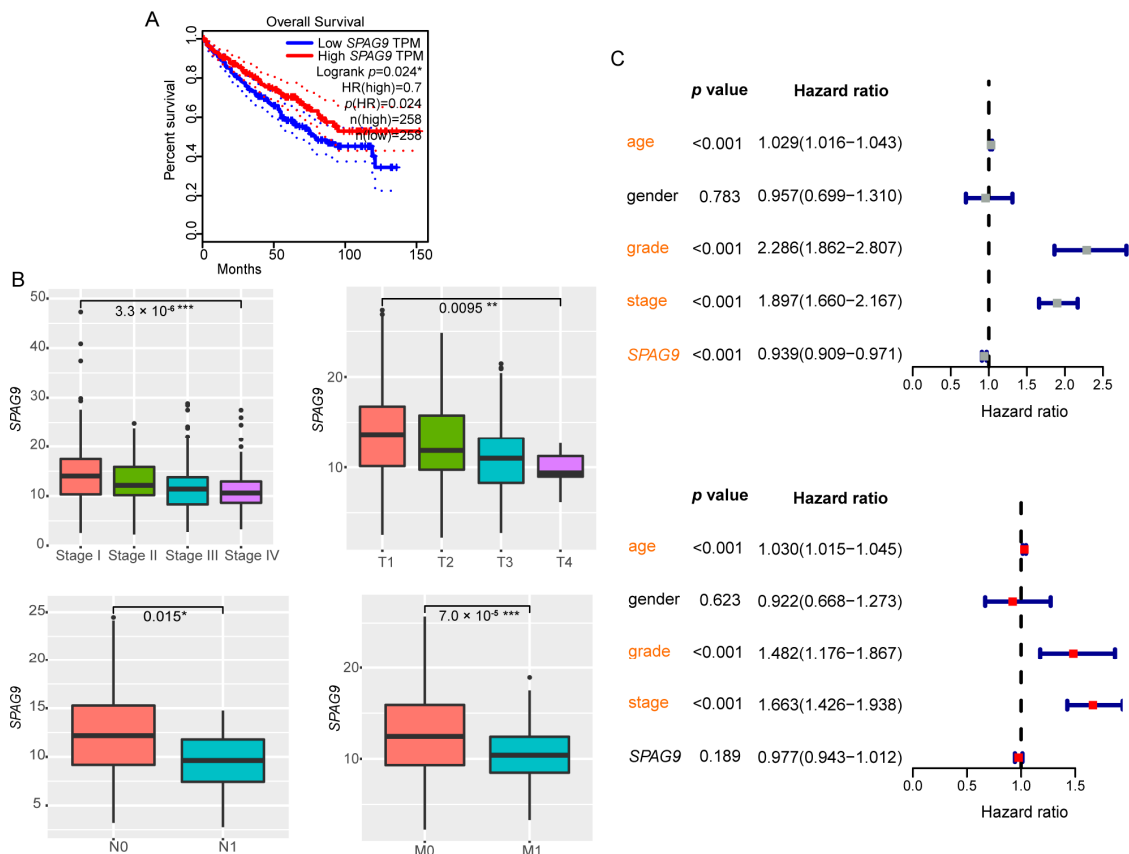


Figure 1. Survival analysis of *SPAG9* in ccRCC. (A) Kaplan–Meier survival analysis of 516 ccRCC patients was performed using GEPIA2 online tool. Median *SPAG9* TPM was chosen as the group cutoff. The 95% CI is shown by the dotted lines. (B) The *SPAG9*-expression differences between stages, T, N, and M in ccRCC patients. Wilcoxon rank-sum test served as the statistical significance test. (C) Univariate (top) and multivariate (bottom) Cox regression analyses of *SPAG9* expression and other clinicopathologic variables in ccRCC. Significant results are marked in orange. * p value < 0.05, ** p value < 0.01, *** p value < 0.001.

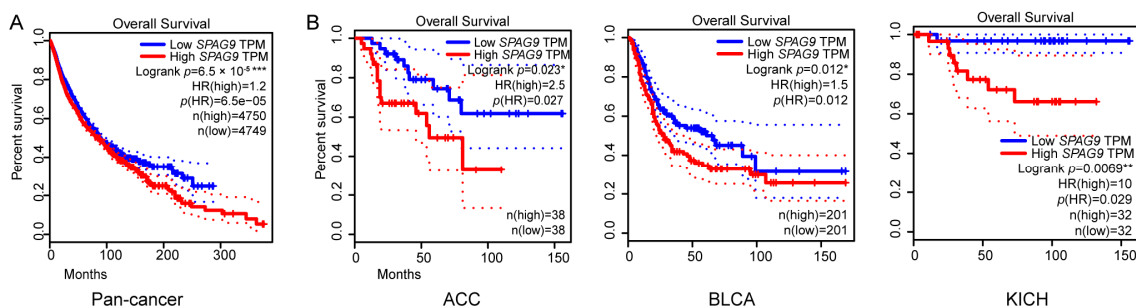


Figure 2. Survival analysis of *SPAG9* in pan-cancer. (A) Using GEPIA2 online tool, Kaplan–Meier survival analysis of 31 kinds of tumor patient, counting up to 9549, was performed. Median *SPAG9* TPM was chosen as the group cutoff. The 95% CI is shown by the dotted lines. (B) Using GEPIA2 online tool, Kaplan–Meier survival analysis was performed on all tumor types except for ccRCC. Only significant results are shown. Abbreviations: ACC, adrenocortical carcinoma; BLCA, bladder urothelial carcinoma; KICH, kidney chromophobe. * p value < 0.05, ** p value < 0.01, *** p value < 0.001.

3.2. *SPAG9* Increases the Expression of Autophagy-Related Genes in 786-O Cells, but Not in HTB-9 Cells

Our study found that *SPAG9* expression predicted opposite clinical outcomes in the pan-cancer and ccRCC patients. To explore the underlying mechanism, we investigated

the roles of *SPAG9* in ccRCC and bladder urothelial carcinoma (BLCA). The latter was chosen for comparison with ccRCC to represent the tumor types in which *SPAG9* expression suggests poor prognosis. The *SPAG9* expression was significantly positively correlated with OS in the ccRCC patients and significantly negatively correlated with OS in the BLCA patients. Previous studies showed that *SPAG9* promotes proliferation and migration in both ccRCC and BLCA cell lines [4,6,14], while *SPAG9* plays opposite prognostic roles in these two cancers. Therefore, we speculated that *SPAG9* participates in other physiological processes in ccRCC.

We carefully reviewed previous studies on the role of *SPAG9* in different tumor-cell lines and summarized the results [4–19] (Table S5). We noted that in addition to promoting proliferation, migration, and EMT, *SPAG9* also promotes autophagy in several tumor-cell lines [18,19]. In ccRCC, increased autophagic flux was reported to be associated with better prognoses [35,36]; therefore, we speculated that *SPAG9* participates in autophagy in ccRCC.

The molecules LC3B, Beclin1, and p62 are landmarks in the autophagic process [37], and the intensity of autophagy was assessed by examining the expression levels of these genes. We overexpressed *SPAG9* in the 786-O cells and HTB-9 cells and detected the expression levels of *MAP1LC3B* (LC3B), *BECN1* (Beclin1), and *SQSTM1* (p62) by RT-qPCR. The overexpression of *SPAG9* significantly increased the *MAP1LC3B*, *BECN1*, and *SQSTM1* mRNA levels in the 786-O cells (Ov-NC vs. Ov-*SPAG9*, p value < 0.05, Figure 3A), but not in the HTB-9 cells (Figure 3B).

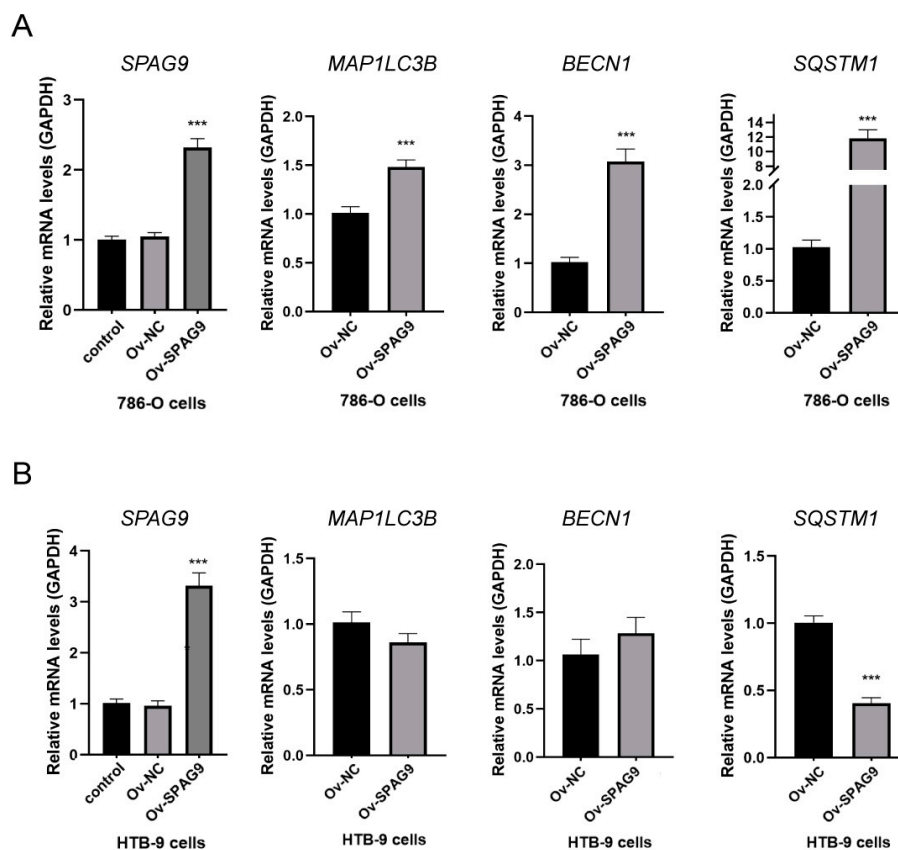


Figure 3. Effects of *SPAG9* overexpression on autophagy-related genes in (A) 786-O cells and (B) HTB-9 cells. Control: untreated cells; Ov-NC: cells transfected with control plasmids; Ov-*SPAG9*: cells transfected with *SPAG9* plasmids. *** p value < 0.001.

3.3. *SPAG9* Expression Was Significantly Correlated with a Weaker Inflammatory Response in ccRCC but Not in BLCA

Previous studies showed that autophagy activation inhibited tumor progression by suppressing the inflammatory response [38], so we investigated the relationship between *SPAG9* and the inflammatory response in ccRCC and BLCA. We used the ssGSEA method to

evaluate the inflammatory response, inflammatory factor production, and T-cell-exhaustion levels in the ccRCC and BLCA samples. As shown in Figure 4, *SPAG9* expression was significantly correlated with a weaker inflammatory response, fewer inflammatory factors, and a lower degree of T-cell exhaustion in ccRCC (lower *SPAG9* expression vs. higher *SPAG9* expression, p value < 0.05, Figure 4A), but not in BLCA (Figure 4B).

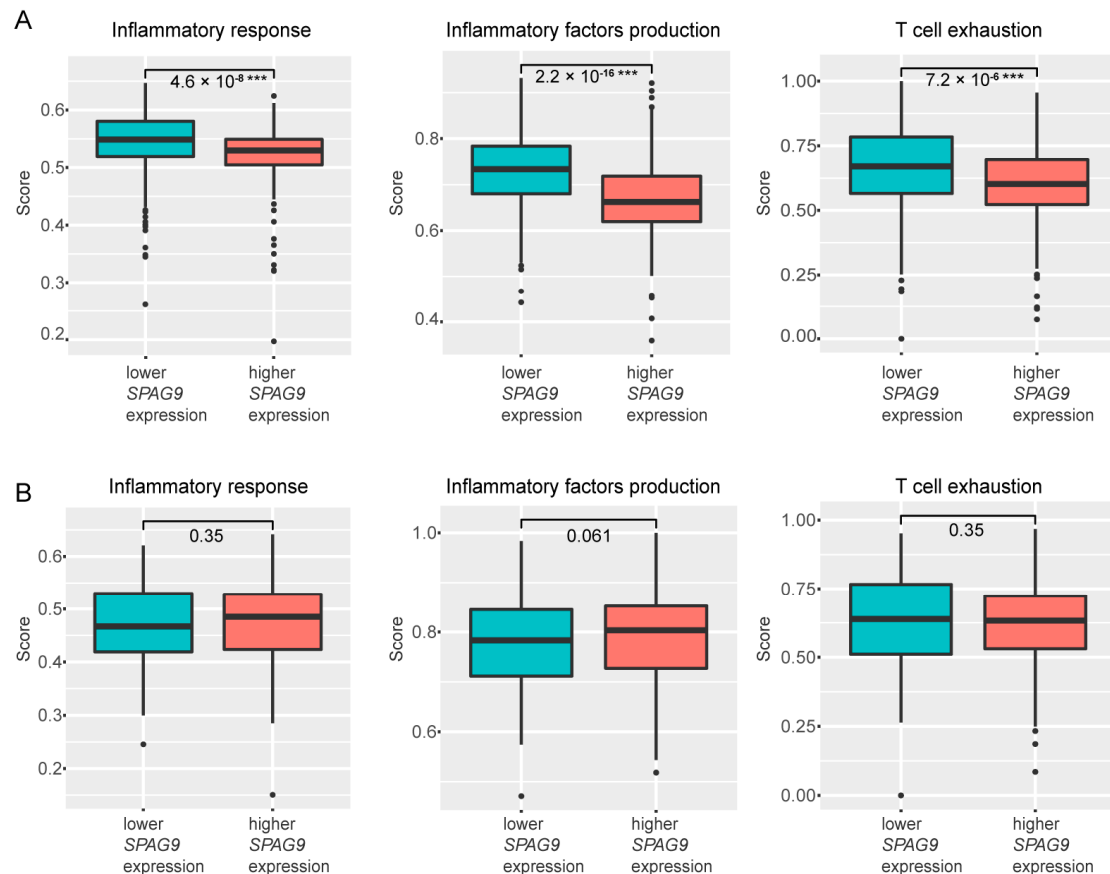


Figure 4. The scores of inflammatory response, inflammatory factor production, and T-cell exhaustion in (A) ccRCC tissues and (B) BLCA tissues with different levels of *SPAG9* expression. Median *SPAG9* expression was chosen as the group cutoff. *** p value < 0.001.

3.4. The Correlation between *SPAG9* Expression and ccRCC Prognosis Depends on the Expression of Key Genes

To further explore the role of *SPAG9* in ccRCC, we calculated the ratio of the immune to the stromal components in the ccRCC samples by using the ESTIMATE algorithm. The ccRCC samples were divided into three groups, based on the median immune and stromal scores: a stroma-rich group (samples with StromalScore > median StromalScore and ImmuneScore < median ImmuneScore), an immunocyte-rich group (samples with StromalScore < median StromalScore and ImmuneScore > median ImmuneScore), and a high-tumor-purity group (samples with StromalScore < median StromalScore and ImmuneScore < median ImmuneScore). A Kaplan–Meier survival analysis was conducted on the three groups, and the *SPAG9* expression was significantly associated with OS only in the stroma-rich group (Figure S1).

Therefore, we performed the following analyses on the stroma-rich group. (1) The samples were divided into two groups based on the median *SPAG9* expression, and GSEA was conducted. As shown in Figure 5A, the genes in the high-*SPAG9*-expression group were significantly enriched in transmembrane signal transduction and phosphorylation regulatory pathways (adipocytokine-signaling pathway, ERBB-signaling pathway, JAK-STAT-signaling pathway, mTOR-signaling pathway, natural-killer-cell-mediated cytotoxicity, neurotrophin-

signaling pathway, phosphatidylinositol-signaling system, and T-cell-receptor-signaling pathway), and the genes in the low-*SPAG9*-expression group were significantly enriched in mitochondrial dysfunction and abnormal calcium signaling pathways (Alzheimer’s disease, cardiac muscle contraction, Huntington’s disease, oxidative phosphorylation, and Parkinson’s disease). (2) Based on the core enrichment genes of each pathway, we used the ssGSEA algorithm to evaluate the pathway activity, and the correlation between the pathway activity and the OS was then calculated. Among the pathways listed above, the activities of the adipocytokine-signaling pathway, ERBB-signaling pathway, and JAK-STAT-signaling pathway were the most strongly correlated with the OS in the ccRCC patients, and these three pathways shared many common core enrichment genes (Figure 5B,C, Table S6). (3) From the common core enrichment genes of these three pathways, seven key genes (*AKT3*, *MAPK8*, *PIK3CA*, *PIK3R3*, *SOS1*, *SOS2*, and *STAT5B*) were screened out, and the expression of these genes had a high correlation with both the *SPAG9* expression and the OS in ccRCC (Figure 5D). The workflow for the screening of these key genes is shown in Table S7. In ccRCC, only the patients with high *SPAG9* expression/high key-gene expression had a better prognosis (Figure 6).

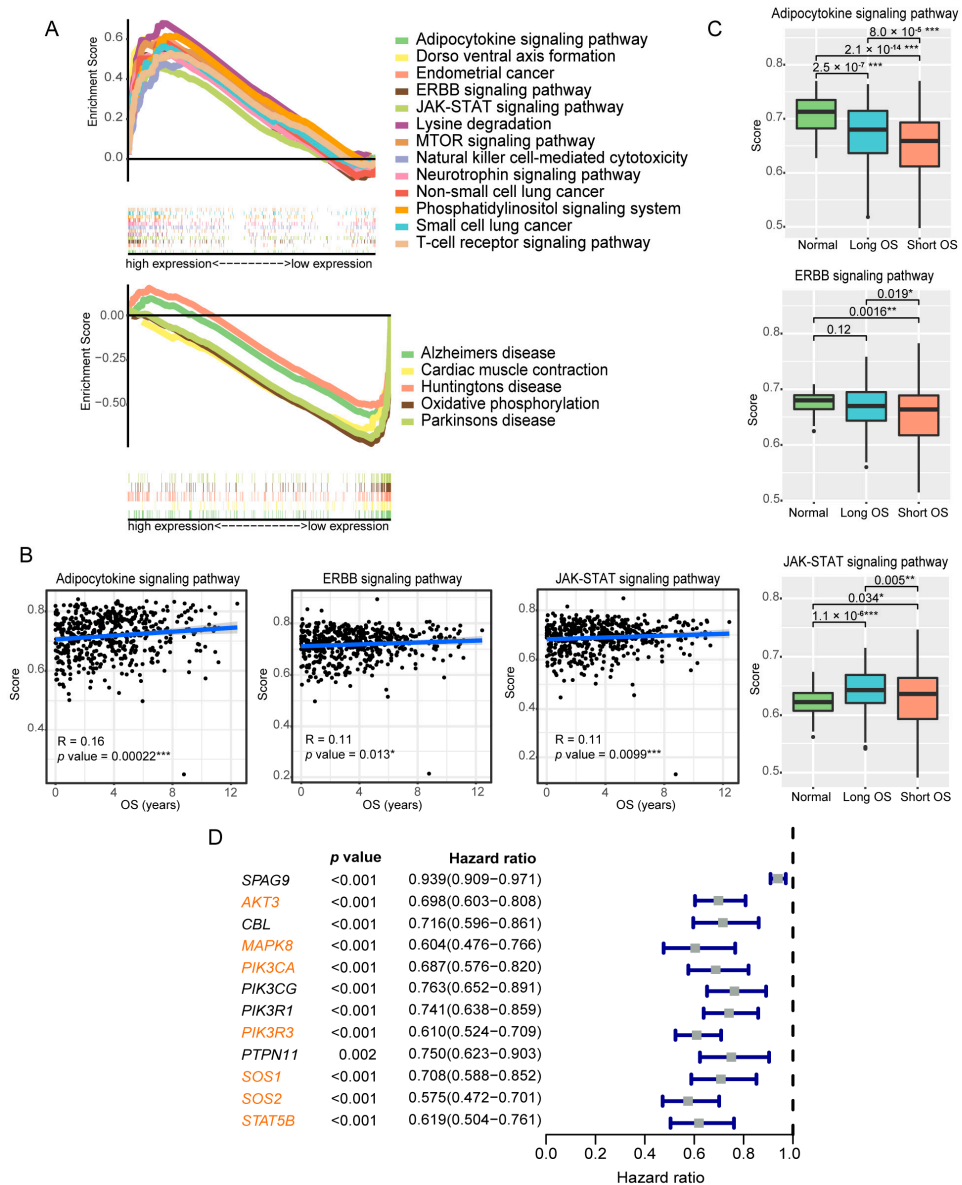


Figure 5. Analysis of the stroma-rich group and key-gene screening. (A) Tissues from the stroma-rich group were divided into two groups based on the median *SPAG9* expression (the high-*SPAG9*-expression

group and the low-*SPAG9*-expression group), and GSEA analysis (in KEGG collection) was conducted, respectively. Each line represents one particular pathway with a unique color. At the bottom, genes up-regulated in a particular pathway are on the left of x-axis; by contrast, the down-regulated genes are on the right. Only pathways with $|NES| > 2$ and FDR p values ≤ 0.05 are shown. Top: the enriched pathways in the high-*SPAG9*-expression group; bottom: the enriched pathways in the low-*SPAG9*-expression group. **(B)** Scatter plots showing the correlation between the activity scores of the adipocytokine-signaling pathway (**left**), ERBB-signaling pathway (**middle**), and JAK-STAT-signaling pathway (**right**) and OS in ccRCC. **(C)** The activity scores of the adipocytokine-signaling pathway (**up**), ERBB-signaling pathway (**middle**), and JAK-STAT-signaling pathway (**down**) in tissues with different levels of malignancy. Normal: ccRCC paracancerous tissues; Long OS: ccRCC tissues from patients with longer OS (OS > median OS); Short OS: ccRCC tissues from patients with shorter OS (OS < median OS). **(D)** Univariate Cox analysis of the expression of *SPAG9* and candidate genes in ccRCC. The selected key genes are marked in orange. * p value < 0.05, ** p value < 0.01, *** p value < 0.001.

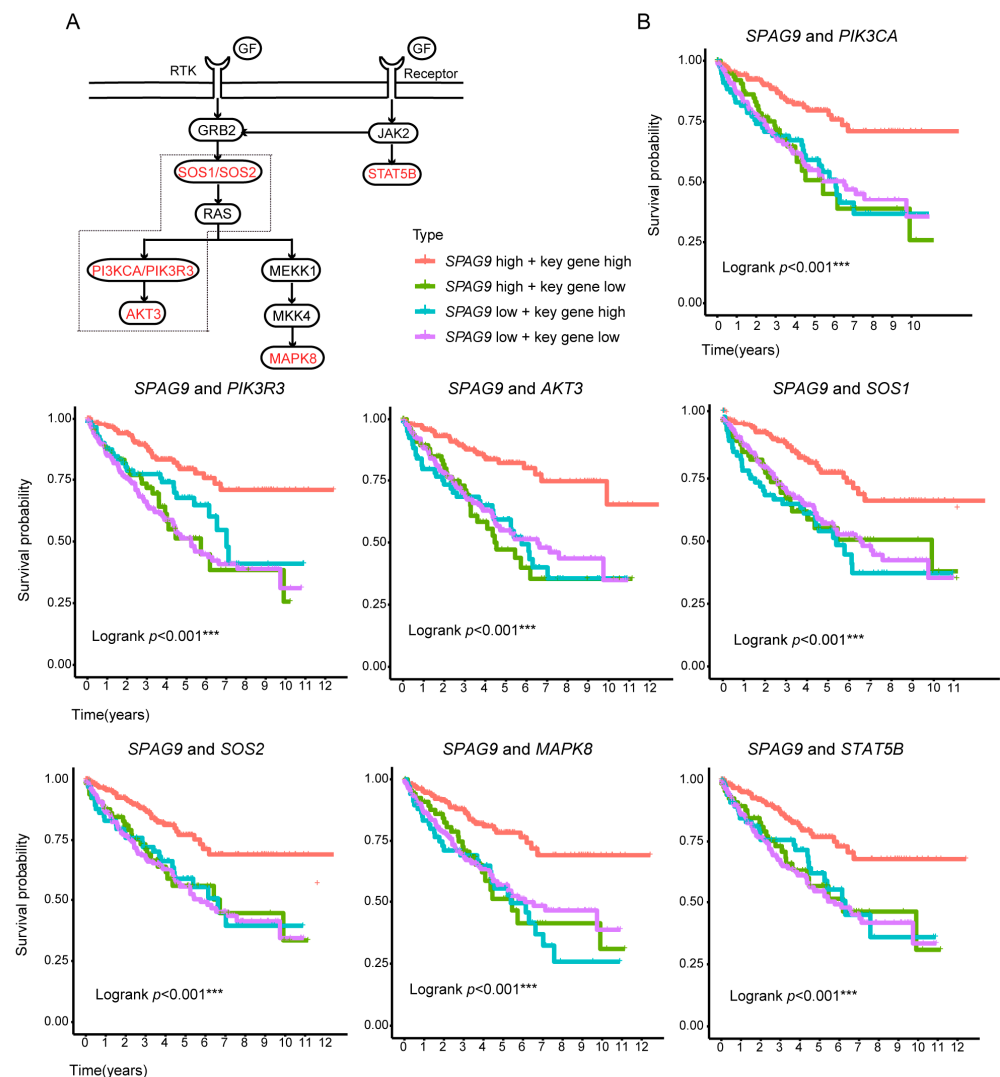


Figure 6. The correlation between *SPAG9* expression and ccRCC prognosis depends on the expression of key genes. **(A)** A signaling diagram collated from KEGG database. Key genes are marked in red. PI3K/AKT-pathway members are depicted by dotted lines. **(B)** Kaplan–Meier survival analysis was conducted on ccRCC patients with different gene-expression combinations (red: high key-gene expression and high *SPAG9* expression; blue: high key-gene expression and low *SPAG9* expression; green: low key-gene expression and high *SPAG9* expression; purple: low key-gene expression and low *SPAG9* expression). *** p value < 0.001.

By analyzing the scRNA-seq data of the ccRCC patients, we found that the key genes were highly expressed in the tumor stromal cells (endothelial cells) (Figure S2), which was consistent with the previous finding that *SPAG9* expression was significantly associated with OS only in the stroma-rich group (Figure S1).

3.5. The Key Genes May Have a Synergistic Effect with *SPAG9* in Terms of Promoting Autophagy

Since most of the key genes belonged to the PI3K-AKT pathway (Figure 6A), to demonstrate the synergistic relationship between *SPAG9* and key genes, the PI3K agonist 740Y-P was used to stimulate the 786-O cells to mimic the effect of key-gene overexpression. The 740Y-P further increased the *MAP1LC3B*, *BECN1*, and *SQSTM1* mRNA levels by more than twofold compared with Ov-*SPAG9* cells (Ov-*SPAG9* + 740Y-P vs. Ov-*SPAG9*, p value < 0.05, Figure 7)

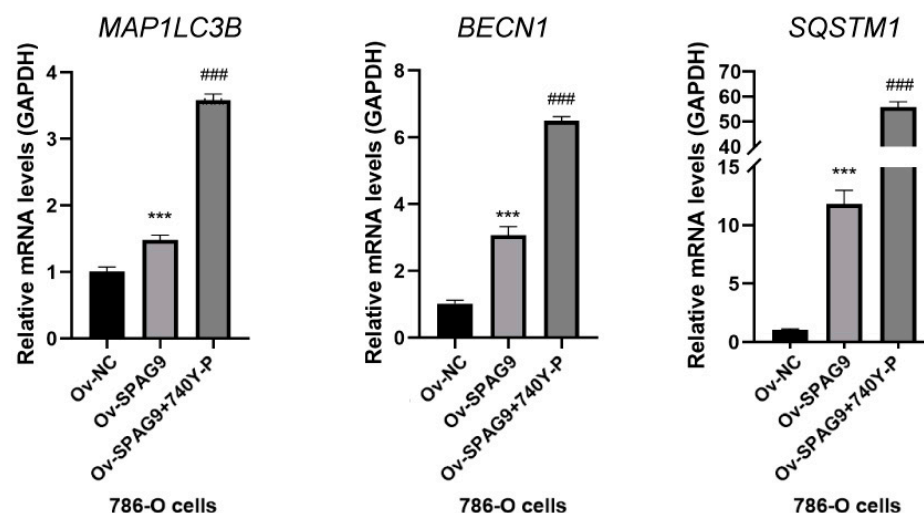


Figure 7. Effects of 740Y-P stimulation on autophagy-related genes in 786-O cells. *** p value < 0.001 vs. Ov-NC; ### p value < 0.001 vs. Ov-*SPAG9*. Ov-NC: cells transfected with control plasmids; Ov-*SPAG9*: cells transfected with *SPAG9* plasmids; Ov-*SPAG9* + 740Y-P: cells transfected with *SPAG9* plasmids and stimulated by 740Y-P.

3.6. Construction and Validation of a *SPAG9*-Based ccRCC Prognostic Model

Based on the expression levels of *SPAG9*/key genes, we constructed a formula for the risk score by lasso regression: RiskScore (RS) = $\text{ExpAKT3} \times (-0.007) + \text{ExpPIK3R3} \times (-0.337) + \text{ExpSOS1} \times 0.196 + \text{ExpSOS2} \times (-0.357) + \text{ExpSTAT5B} \times (-0.001)$. Next, we integrated age, gender, and RiskScore to construct a nomogram to predict the survival probability of the ccRCC patients (Figure 8A). The calibration curves showed good agreement between the predicted 1-, 3-, and 5-year survival rates and the respective actual survival rates (Figure 8B).

The predictive power of the nomogram was validated using C-indexes and ROC curves. The C-indexes of the nomogram were higher than 0.6 in both the training cohort and the validation cohort, and they were higher for the patients with shorter disease courses (Figure 9A). The ROC analysis indicated that the nomogram had some predictive value in both the training cohort and the validation cohort, especially in the patients with a 1-year disease course (in the training cohort: AUC at 1 years = 0.708, AUC at 3 years = 0.675, AUC at 5 years = 0.686; in the validation cohort: AUC at 1 years = 0.672, AUC at 3 years = 0.657, AUC at 5 years = 0.625, Figure 9B).

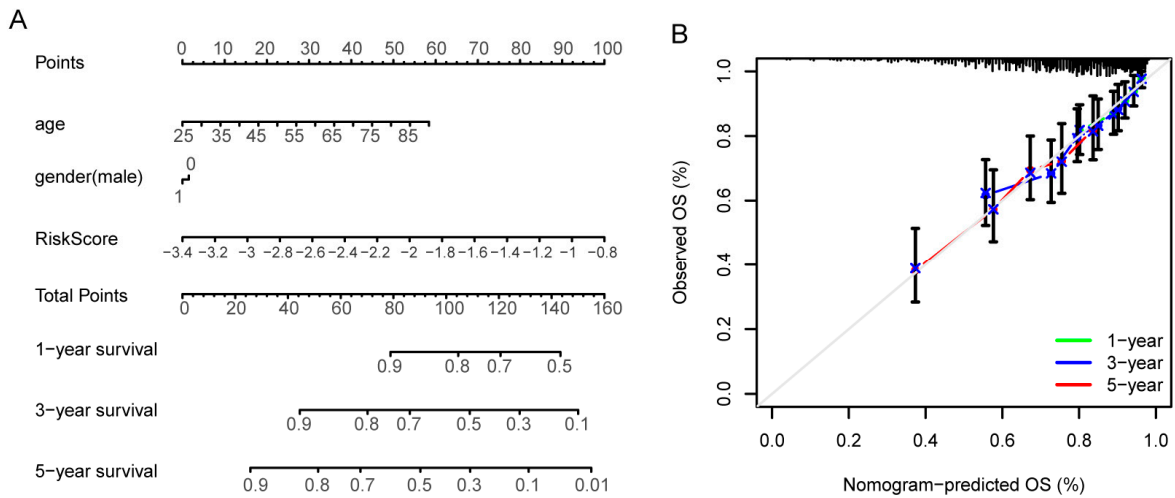


Figure 8. Construction of the *SPAG9*-based ccRCC prognostic model. (A) A nomogram to predict the prognoses of ccRCC patients, containing age, gender, and risk score. Total Points = $(0.899 \times \text{age} - 22.468) + (-1.508 \times \text{gender} + 1.508) + (38.462 \times \text{RiskScore} + 130.769)$. (B) Calibration plots of the nomogram for predicting OS at 1-, 3-, and 5-year survival rates. T, actual survival proportion, is plotted on the y-axis with 95% confidence. Nomogram-predicted survival probability is plotted on the x-axis. The gray line is an ideal curve, with a slope of 1.

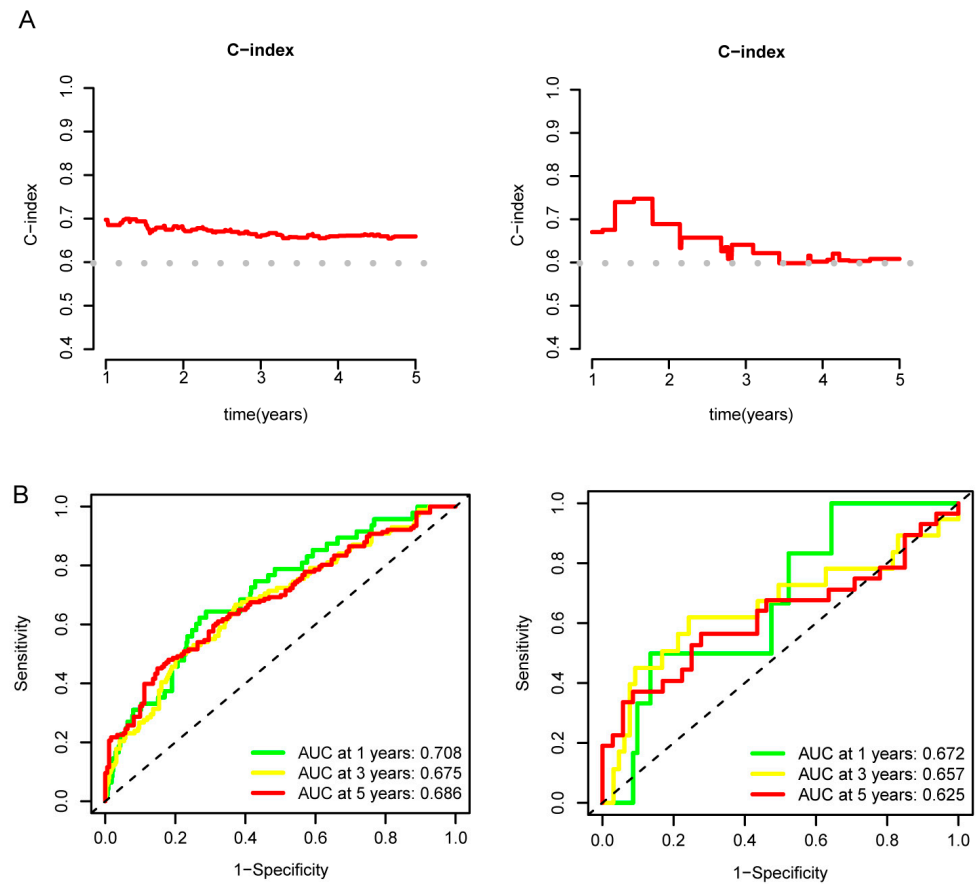


Figure 9. Validation of the *SPAG9*-based ccRCC prognostic model. (A) Time-dependent C-indexes of the nomogram in the training cohort (left) and validation cohort (right). The dotted lines were set at C-index = 0.6. (B) The ROC curves of the nomogram in the training cohort (left) and validation cohort (right). The dotted lines were reference lines, ROC curves under the reference line had no diagnostic value.

4. Discussion

It was reported that *SPAG9* promotes proliferation and migration in many tumor-cell lines, including the ccRCC cell lines Caki-1 and NII-AKS413 [4]. However, we found that *SPAG9* was associated with good prognosis in ccRCC patients, which contrasted with its widely recognized cancer-promoting role and was not found in other tumors. Thus, we speculated that *SPAG9* participates in other physiological processes in ccRCC.

We summarized the roles of *SPAG9* in tumor-cell lines and noted that in addition to promoting proliferation, migration, and EMT [4–17], *SPAG9* also promotes autophagy in several tumor-cell lines [18,19]. Autophagy is a cellular degradation pathway for macromolecular substances. Cells initiate autophagy after they are stimulated by external stress, and misfolded proteins and damaged organelles are engulfed by autophagic vesicles and lysosomes [37]. Autophagy has a dual effect in tumors: in the early stage, autophagy inhibits tumorigenesis by inhibiting the destruction of the genome by the reactive oxygen species produced by damaged mitochondria. In the late stage, autophagy helps tumor cells survive hypoxia and a lack of nutrients [38–40].

In ccRCC, Radovanovic et al. found that an increase in autophagic flux was associated with a lower tumor stage, reduced metastasis, and an improved 5-year survival rate [36]. Xu also found that the autophagy-promoting gene MAP1S was associated with better prognoses in ccRCC patients [35]. In ccRCC, studies reported that the activation of autophagy effectively inhibits tumor progression [41,42]. Moreover, prognostic models based on autophagy have also been widely developed and proven to have good predictive value [43–47]. Thus, autophagy may play an important role in ccRCC and, overall, it has a protective effect.

Autophagy inhibits inflammatory responses by inhibiting oxidative stress and lysosomal rupture [38]. Inflammation plays an important role in tumor progression: inflammatory responses stimulate tumor-associated macrophages to secrete cytokines, such as TGF- β and TNF- α , and promote tumor-cell metastasis; a persistent inflammatory response also leads to T-cell exhaustion and further tumor progression [22]. Clear-cell renal cell carcinoma is a tumor type with a high degree of immune infiltration [1]. The activation of autophagy in ccRCC may reduce the pro-inflammatory stress from tumor cells to the surrounding immune cells, inhibit tumor progression, and prolong the survival times of patients.

Therefore, we hypothesized that *SPAG9* suppresses tumor progression by promoting autophagy in ccRCC. We found that the overexpression of *SPAG9* significantly increased the mRNA levels of autophagy-associated genes in the 786-O cells but not in the HTB-9 cells. Moreover, the *SPAG9* expression was significantly correlated with weaker inflammatory responses, fewer inflammatory factors, and a lower degree of T-cell exhaustion in ccRCC, but not in BLCA. Based on this information, we established a possible mechanism through which *SPAG9* affects the prognosis of patients with ccRCC and BLCA: in ccRCC, *SPAG9* promotes tumor growth but also promotes autophagy and inhibits the inflammatory response, and it has a protective effect on the whole; in BLCA, *SPAG9* promotes tumor growth and leads to poor prognoses.

Through further analyses, we found that the correlation between *SPAG9* expression and ccRCC prognosis was dependent on the tumor stroma. By analyzing stroma-rich samples, we identified seven key genes (*AKT3*, *MAPK8*, *PIK3CA*, *PIK3R3*, *SOS1*, *SOS2*, and *STAT5B*) in this study. In ccRCC, *SPAG9* expression was significantly associated with OS only when key genes were highly expressed. The scRNA-seq data further proved that the key genes were highly expressed in the tumor stroma of ccRCC. Since most of the key genes were PI3K-AKT-pathway members, we used the PI3K agonist 740Y-P to stimulate the 786-O cells to mimic the effect of key-gene overexpression. Furthermore, the addition of 740Y-P significantly increased the expression of the autophagy-related genes by more than twofold compared with the Ov-*SPAG9* cells. In conclusion, we speculated that in the tumor stroma, some genes cooperate with *SPAG9* to promote autophagy, and that these may be key genes, which can be represented by the key genes.

Finally, we constructed a nomogram based on the *SPAG9*/key genes and other clinical features to predict survival in the ccRCC patients. Combined with external data validation, the nomogram proved to have some predictive value. The estimation of the long-term prognosis of ccRCC patients can help physicians develop individualized treatment plans [48]. With this new nomogram, we look forward to providing more helpful guidance for clinical work.

5. Conclusions

In recent years, research on the role of *SPAG9* in tumors has mainly focused on its role in promoting tumor progression [49], but our study found that *SPAG9* expression was significantly associated with good prognoses in ccRCC, a result that has not been found in other cancer types and contradicts the widely recognized cancer-promoting role of *SPAG9*. Combined with a bioinformatics analysis and an experimental validation, we speculated that *SPAG9* suppresses tumor progression by promoting autophagy and inhibiting inflammatory responses in ccRCC. We further found that some genes might cooperate with *SPAG9* to promote autophagy, and that these were highly expressed in the tumor stroma and may be key genes. Finally we constructed a nomogram based on *SPAG9*/key genes and other clinical features, which was proven to have some predictive value.

Supplementary Materials: The following supporting information can be downloaded at: <https://www.mdpi.com/article/10.3390/genes14040944/s1>. Figure S1: *SPAG9* expression is significantly associated with OS only in the stroma-rich group. Figure S2: The key genes are highly expressed in ccRCC stromal cells. Table S1: Baseline clinical characteristics of ccRCC patients from the TCGA database. Table S2: Baseline clinical characteristics of ccRCC patients from the ICGC database. Table S3: Primers designed for this study. Table S4: The qPCR data after analysis with $2^{-\Delta\Delta C_t}$ method. Table S5: The role of *SPAG9* in different tumor-cell lines; Table S6: The correlation between the activity scores of pathways and OS in ccRCC. Table S7: Workflow for screening of key genes.

Author Contributions: Conceptualization, writing—review and editing, validation, and funding acquisition: H.W.; methodology, software, formal analysis, investigation, resources, data curation, writing—original draft preparation, and visualization: L.Q. Funding acquisition and project administration: L.Z. All authors have read and agreed to the published version of the manuscript.

Funding: This work was supported by the following grants: from the National Natural Science Foundation of China (NSFC), awarded to H.W. (no. 82270711) and L.Z. (no. 81800614); from Hubei Province Major Scientific and Technological Special Project, awarded to H.W. (no. 2019ACA137); and from China Population Welfare Foundation, awarded to H.W. (no. SLB-6-20210323-99).

Institutional Review Board Statement: Not applicable.

Informed Consent Statement: Not applicable.

Data Availability Statement: The data that support the findings of this study are openly available on the TCGA database and the GEO database.

Conflicts of Interest: The authors declare no conflict of interest.

References

1. Hsieh, J.J.; Purdue, M.P.; Signoretti, S.; Swanton, C.; Albiges, L.; Schmidinger, M.; Heng, D.Y.; Larkin, J.; Ficarra, V. Renal Cell Carcinoma. *Nat. Rev. Dis. Prim.* **2017**, *3*, 17009. [[CrossRef](#)] [[PubMed](#)]
2. Siegel, R.L.; Miller, K.D.; Fuchs, H.E.; Jemal, A. Cancer Statistics, 2021. *CA A Cancer J. Clin.* **2021**, *71*, 7–33. [[CrossRef](#)]
3. Khattak, M.; Larkin, J. Sequential Therapy with Targeted Agents in Metastatic Renal Cell Carcinoma: Beyond Second-Line and Overcoming Drug Resistance. *World J. Urol.* **2014**, *32*, 19–29. [[CrossRef](#)] [[PubMed](#)]
4. Garg, M.; Kanojia, D.; Khosla, A.; Dudha, N.; Sati, S.; Chaurasiya, D.; Jagadish, N.; Seth, A.; Kumar, R.; Gupta, S.; et al. Sperm-Associated Antigen 9 is Associated with Tumor Growth, Migration, and Invasion in Renal Cell Carcinoma. *Cancer Res.* **2008**, *68*, 8240–8248. [[CrossRef](#)]
5. Kanojia, D.; Garg, M.; Gupta, S.; Gupta, A.; Suri, A. Sperm-Associated Antigen 9 Is a Novel Biomarker for Colorectal Cancer and is Involved in Tumor Growth and Tumorigenicity. *Am. J. Pathol.* **2011**, *178*, 1009–1020. [[CrossRef](#)] [[PubMed](#)]
6. Kanojia, D.; Garg, M.; Saini, S.; Agarwal, S.; Parashar, D.; Jagadish, N.; Seth, A.; Bhatnagar, A.; Gupta, A.; Kumar, R.; et al. Sperm Associated Antigen 9 Plays an Important Role in Bladder Transitional Cell Carcinoma. *PLoS ONE* **2013**, *8*, e81348. [[CrossRef](#)] [[PubMed](#)]

7. Chen, F.; Lu, Z.; Deng, J.; Han, X.; Bai, J.; Liu, Q.; Xi, Y.; Zheng, J. SPAG9 Expression is Increased in Human Prostate Cancer and Promotes Cell Motility, Invasion and Angiogenesis In Vitro. *Oncol. Rep.* **2014**, *32*, 2533–2540. [[CrossRef](#)]
8. Miao, Z.F.; Wang, Z.N.; Zhao, T.T.; Xu, Y.Y.; Wu, J.H.; Liu, X.Y.; Xu, H.; You, Y.; Xu, H.M. Overexpression of SPAG9 in Human Gastric Cancer is Correlated with Poor Prognosis. *Virchows Arch.* **2015**, *467*, 525–533. [[CrossRef](#)]
9. Ha, J.H.; Yan, M.; Gomathinayagam, R.; Jayaraman, M.; Husain, S.; Liu, J.; Mukherjee, P.; Reddy, E.P.; Song, Y.S.; Dhanasekaran, D.N. Aberrant Expression of JNK-Associated Leucine-Zipper Protein, JLP, Promotes Accelerated Growth of Ovarian Cancer. *Oncotarget* **2016**, *7*, 72845–72859. [[CrossRef](#)]
10. Jagadish, N.; Gupta, N.; Agarwal, S.; Parashar, D.; Sharma, A.; Fatima, R.; Topno, A.P.; Kumar, V.; Suri, A. Sperm-Associated Antigen 9 (Spag9) Promotes the Survival and Tumor Growth of Triple-Negative Breast Cancer Cells. *Tumour Biol.* **2016**, *37*, 13101–13110. [[CrossRef](#)]
11. Xiao, C.; Fu, L.; Yan, C.; Shou, F.; Liu, Q.; Li, L.; Cui, S.; Duan, J.; Jin, G.; Chen, J.; et al. SPAG9 is Overexpressed in Osteosarcoma, and Regulates Cell Proliferation and Invasion through Regulation of JunD. *Oncol. Lett.* **2016**, *12*, 2674–2679. [[CrossRef](#)]
12. Yang, X.; Zhou, W.; Liu, S. Spag9 Controls the Cell Motility, Invasion and Angiogenesis of Human Osteosarcoma Cells. *Exp. Ther. Med.* **2016**, *11*, 637–644. [[CrossRef](#)] [[PubMed](#)]
13. Jagadish, N.; Fatima, R.; Sharma, A.; Devi, S.; Suri, V.; Kumar, V.; Suri, A. Sperm Associated Antigen 9 (SPAG9) a Promising Therapeutic Target of Ovarian Carcinoma. *Tumour Biol.* **2018**, *40*, 1010428318773652. [[CrossRef](#)]
14. Li, X.; Jiang, F.; Wang, X.; Gu, X. Spag9 regulates HGF1 Expression and Drives EMT in Bladder Transitional Cell Carcinoma via rac1 Signaling Pathway. *Am. J. Cancer Res.* **2018**, *8*, 2467–2480.
15. Ren, B.; Zou, G.; He, J.; Huang, Y.; Ma, G.; Xu, G.; Li, Y.; Yu, P. Sperm-Associated antigen 9 is Upregulated in Hepatocellular Carcinoma Tissue and Enhances QGY cell Proliferation and Invasion In Vitro. *Oncol. Lett.* **2018**, *15*, 415–422. [[CrossRef](#)] [[PubMed](#)]
16. Luo, S.; Ren, B.; Zou, G.; Liu, J.; Chen, W.; Huang, Y.; Chen, X.; Fu, Y. SPAG9/MKK3/p38 axis Is a Novel Therapeutic Target for Liver Cancer. *Oncol. Rep.* **2019**, *41*, 2329–2336. [[CrossRef](#)]
17. Xiao, C.; Li, M.; Huang, Q.; Si-Tu, J. SPAG9 Promotes Prostate Cancer Proliferation and Metastasis via MAPK Signaling Pathway. *Am. J. Transl. Res.* **2019**, *11*, 5249–5260.
18. Boldbaatar, J.; Gunarta, I.K.; Suzuki, R.; Erdenebaatar, P.; Davaakhuu, G.; Hohjoh, H.; Yoshioka, K. Protective Role of c-Jun NH(2)-Terminal Kinase-Associated Leucine Zipper Protein (JLP) in Curcumin-Induced Cancer Cell Death. *Biochem. Biophys. Res. Commun.* **2020**, *522*, 697–703. [[CrossRef](#)] [[PubMed](#)]
19. Suzuki, R.; Gunarta, I.K.; Boldbaatar, J.; Erdenebaatar, P.; Odongoo, R.; Yoshioka, K. Functional role of c-Jun NH(2)-Terminal Kinase-Associated Leucine Zipper Protein (JLP) in Lysosome Localization and Autophagy. *Drug Discov. Ther.* **2020**, *14*, 35–41. [[CrossRef](#)]
20. Su, C.; Lv, Y.; Lu, W.; Yu, Z.; Ye, Y.; Guo, B.; Liu, D.; Yan, H.; Li, T.; Zhang, Q.; et al. Single-Cell RNA Sequencing in Multiple Pathologic Types of Renal Cell Carcinoma Revealed Novel Potential Tumor-Specific Markers. *Front. Oncol.* **2021**, *11*, 719564. [[CrossRef](#)] [[PubMed](#)]
21. Tang, Z.; Kang, B.; Li, C.; Chen, T.; Zhang, Z. GEPIA2: An Enhanced Web Server for Large-Scale Expression Profiling and Interactive Analysis. *Nucleic Acids Res.* **2019**, *47*, W556–W560. [[CrossRef](#)]
22. Terlizzi, M.; Casolaro, V.; Pinto, A.; Sorrentino, R. Inflammasome: Cancer's Friend or Foe? *Pharmacol. Ther.* **2014**, *143*, 24–33. [[CrossRef](#)]
23. Zheng, L.; Qin, S.; Si, W.; Wang, A.; Xing, B.; Gao, R.; Ren, X.; Wang, L.; Wu, X.; Zhang, J.; et al. Pan-Cancer Single-Cell Landscape of Tumor-Infiltrating T cells. *Science* **2021**, *374*, abe6474. [[CrossRef](#)] [[PubMed](#)]
24. Mootha, V.K.; Lindgren, C.M.; Eriksson, K.F.; Subramanian, A.; Sihag, S.; Lehar, J.; Puigserver, P.; Carlsson, E.; Ridderstråle, M.; Laurila, E.; et al. PGC-1alpha-Responsive Genes Involved in Oxidative Phosphorylation are Coordinately Downregulated in Human Diabetes. *Nat. Genet.* **2003**, *34*, 267–273. [[CrossRef](#)]
25. Subramanian, A.; Tamayo, P.; Mootha, V.K.; Mukherjee, S.; Ebert, B.L.; Gillette, M.A.; Paulovich, A.; Pomeroy, S.L.; Golub, T.R.; Lander, E.S.; et al. Gene Set Enrichment Analysis: A Knowledge-Based Approach for Interpreting Genome-Wide Expression Profiles. *Proc. Natl. Acad. Sci. USA* **2005**, *102*, 15545–15550. [[CrossRef](#)] [[PubMed](#)]
26. Yoshihara, K.; Shahmoradgoli, M.; Martínez, E.; Vegesna, R.; Kim, H.; Torres-Garcia, W.; Treviño, V.; Shen, H.; Laird, P.W.; Levine, D.A.; et al. Inferring Tumour Purity and Stromal and Immune Cell Admixture from Expression Data. *Nat. Commun.* **2013**, *4*, 2612. [[CrossRef](#)]
27. Lall, S.; Sinha, D.; Bandyopadhyay, S.; Sengupta, D. Structure-Aware Principal Component Analysis for Single-Cell RNA-seq Data. *J. Comput. Biol.* **2018**, *25*, 1365–1373. [[CrossRef](#)] [[PubMed](#)]
28. Satija, R.; Farrell, J.A.; Gennert, D.; Schier, A.F.; Regev, A. Spatial Reconstruction of Single-Cell Gene Expression Data. *Nat. Biotechnol.* **2015**, *33*, 495–502. [[CrossRef](#)]
29. Aran, D.; Looney, A.P.; Liu, L.; Wu, E.; Fong, V.; Hsu, A.; Chak, S.; Naikawadi, R.P.; Wolters, P.J.; Abate, A.R.; et al. Reference-based Analysis of Lung Single-Cell Sequencing Reveals a Transitional Profibrotic Macrophage. *Nat. Immunol.* **2019**, *20*, 163–172. [[CrossRef](#)]
30. Ward-Peterson, M.; Maziak, W. For Smoking Cessation, E-Cigarette Flavors Aren't Required. *Nicotine Tob. Res.* **2019**, *21*, 132–133. [[CrossRef](#)]
31. Qiu, X.; Mao, Q.; Tang, Y.; Wang, L.; Chawla, R.; Pliner, H.A.; Trapnell, C. Reversed Graph Embedding Resolves Complex Single-Cell Trajectories. *Nat. Methods* **2017**, *14*, 979–982. [[CrossRef](#)] [[PubMed](#)]

32. Nagashima, K.; Sato, Y. Information Criteria for Firth's Penalized Partial Likelihood Approach in Cox Regression Models. *Stat. Med.* **2017**, *36*, 3422–3436. [[CrossRef](#)] [[PubMed](#)]
33. Wang, Z.; Gao, L.; Guo, X.; Feng, C.; Lian, W.; Deng, K.; Xing, B. Development and Validation of a Nomogram with an Autophagy-Related Gene Signature for Predicting Survival in Patients with Glioblastoma. *Aging* **2019**, *11*, 12246–12269. [[CrossRef](#)]
34. Alba, A.C.; Agoritsas, T.; Walsh, M.; Hanna, S.; Iorio, A.; Devereaux, P.J.; McGinn, T.; Guyatt, G. Discrimination and Calibration of Clinical Prediction Models: Users' Guides to the Medical Literature. *JAMA* **2017**, *318*, 1377–1384. [[CrossRef](#)]
35. Xu, G.; Jiang, Y.; Xiao, Y.; Liu, X.D.; Yue, F.; Li, W.; Li, X.; He, Y.; Jiang, X.; Huang, H.; et al. Fast Clearance of Lipid Droplets through MAP1S-Activated Autophagy Suppresses Clear Cell Renal Cell Carcinomas and Promotes Patient Survival. *Oncotarget* **2016**, *7*, 6255–6265. [[CrossRef](#)]
36. Radovanovic, M.; Vidicevic, S.; Tasic, J.; Tomonjic, N.; Stanojevic, Z.; Nikic, P.; Vuksanovic, A.; Dzamic, Z.; Bumbasirevic, U.; Isakovic, A.; et al. Role of AMPK/mTOR-Independent autophagy in Clear Cell Renal Cell Carcinoma. *J. Investig. Med.* **2020**, *68*, 1386–1393. [[CrossRef](#)]
37. Levine, B.; Kroemer, G. Biological Functions of Autophagy Genes: A Disease Perspective. *Cell* **2019**, *176*, 11–42. [[CrossRef](#)]
38. Zhong, Z.; Sanchez-Lopez, E.; Karin, M. Autophagy, Inflammation, and Immunity: A Troika Governing Cancer and Its Treatment. *Cell* **2016**, *166*, 288–298. [[CrossRef](#)]
39. Kimmelman, A.C.; White, E. Autophagy and Tumor Metabolism. *Cell Metab.* **2017**, *25*, 1037–1043. [[CrossRef](#)] [[PubMed](#)]
40. Amaravadi, R.K.; Kimmelman, A.C.; Debnath, J. Targeting Autophagy in Cancer: Recent Advances and Future Directions. *Cancer Discov.* **2019**, *9*, 1167–1181. [[CrossRef](#)]
41. Xiao, W.; Xiong, Z.; Xiong, W.; Yuan, C.; Xiao, H.; Ruan, H.; Song, Z.; Wang, C.; Bao, L.; Cao, Q.; et al. Melatonin/PGC1A/UCP1 Promotes Tumor Slimming and Represses Tumor Progression by Initiating Autophagy and Lipid Browning. *J. Pineal Res.* **2019**, *67*, e12607. [[CrossRef](#)] [[PubMed](#)]
42. Choi, M.E. Autophagy in Kidney Disease. *Annu. Rev. Physiol.* **2020**, *82*, 297–322. [[CrossRef](#)] [[PubMed](#)]
43. Yang, H.; Han, M.; Li, H. Construction and Validation of an Autophagy-Related Prognostic Risk Signature for Survival Predicting in Clear Cell Renal Cell Carcinoma Patients. *Front. Oncol.* **2020**, *10*, 707. [[CrossRef](#)] [[PubMed](#)]
44. Gui, C.P.; Cao, J.Z.; Tan, L.; Huang, Y.; Tang, Y.M.; Li, P.J.; Chen, Y.H.; Lu, J.; Yao, H.H.; Chen, Z.H.; et al. A Panel of Eight Autophagy-Related Long Non-Coding RNAs Is a Good Predictive Parameter for Clear Cell Renal Cell Carcinoma. *Genomics* **2021**, *113*, 740–754. [[CrossRef](#)]
45. He, M.; Li, M.; Guan, Y.; Wan, Z.; Tian, J.; Xu, F.; Zhou, H.; Gao, M.; Bi, H.; Chong, T. A New Prognostic Risk Score: Based on the Analysis of Autophagy-Related Genes and Renal Cell Carcinoma. *Front. Genet.* **2021**, *12*, 820154. [[CrossRef](#)]
46. Li, X.; Yu, H.; Wei, Z.; Gou, X.; Liang, S.; Liu, F. A Novel Prognostic Model Based on Autophagy-Related Long Non-Coding RNAs for Clear Cell Renal Cell Carcinoma. *Front. Oncol.* **2021**, *11*, 711736. [[CrossRef](#)]
47. Xuan, Y.; Chen, W.; Liu, K.; Gao, Y.; Zuo, S.; Wang, B.; Ma, X.; Zhang, X. A Risk Signature with Autophagy-Related Long Noncoding RNAs for Predicting the Prognosis of Clear Cell Renal Cell Carcinoma: Based on the TCGA Database and Bioinformatics. *Dis. Mkr.* **2021**, *2021*, 8849977. [[CrossRef](#)]
48. Saeed, M.; Khalid, H.; Thakur, S.; Efferth, T. Protein Expression Profiling and Virtual Drug Screening as an Approach for Individualized Therapy of Small Cell Vaginal Carcinoma. *Cancer Genom. Proteom.* **2022**, *19*, 512–525. [[CrossRef](#)]
49. Pan, J.; Yu, H.; Guo, Z.; Liu, Q.; Ding, M.; Xu, K.; Mao, L. Emerging role of sperm-associated antigen 9 in tumorigenesis. *Biomed. Pharmacother.* **2018**, *103*, 1212–1216. [[CrossRef](#)]

Disclaimer/Publisher's Note: The statements, opinions and data contained in all publications are solely those of the individual author(s) and contributor(s) and not of MDPI and/or the editor(s). MDPI and/or the editor(s) disclaim responsibility for any injury to people or property resulting from any ideas, methods, instructions or products referred to in the content.